

Role of Interface Chemistry in Opening New Radiative Pathways in InP/CdSe Giant Quantum Dots with Blinking-Suppressed Two-Color Emission

Allison M. Dennis, Matthew R. Buck, Feng Wang, Nicolai F. Hartmann, Somak Majumder, Joanna L. Casson, John D. Watt, Stephen K. Doorn, Han Htoon, Milan Sykora, and Jennifer A. Hollingsworth*

InP/CdSe core/thick-shell “giant” quantum dots (gQDs) that exhibit blinking-suppressed two-color excitonic emission have been synthesized and optically characterized. These type II heterostructures exhibit photoluminescence from both a charge-separated, near-infrared type II excitonic state, and a shell-localized visible-color excitonic state. Infrared emission is intrinsic to the type II QD, while visible emission can either be eliminated or enhanced through chemical modification of the InP surface prior to CdSe shell growth. Single-QD photoluminescence measurements confirm that the dual color emission is from individual nanocrystals. The probability of observing dual emission from individual QDs and the extent of blinking suppression increases with shell thickness. Visible emission can be stabilized by the addition of a second shell of CdS, where the resulting InP/CdSe/CdS core/shell/shell nanocrystals afford the strongest blinking suppression, determined by analysis of the Mandel Q parameter. Transient absorption spectroscopy verifies that dual emission arises when hole relaxation from the shell to the core is impeded, possibly as a result of enhanced interfacial hole trapping at F[−] or O^{2−} defect sites. Electron–hole recombination in the shell then competes with slower type II recombination, providing a different mechanism for breaking Kasha’s rule and allowing two colors of light to be emitted from one nanostructure.


core semiconductor.^[1] The added shell passivates surface dangling bonds and can create a physical and energetic barrier between the core and the surface. These attributes have the effect of promoting radiative recombination of excited-state carriers in the core by reducing interactions with trap states at the QD surface that otherwise lead to non-radiative recombination. A shell can also serve as a light harvesting component, funneling excitons (bound electron–hole pairs) to the emissive core and effectively increasing the core cross-section without an increase in the size of the core itself.^[2] Further, as the core/shell interface is a semiconductor heterojunction, judicious choice of core and shell materials is a route to nanoscale bandgap engineering that is beyond what can be achieved by quantum size effects alone. In particular, a type II (staggered) alignment of core/shell conduction and valence band energy levels can be used to separate electrons and holes into different regions of the nanocrystal heterostructure

1. Introduction

Core/shell heterostructuring of semiconductor quantum dots (QDs) provides a convenient platform for synthetically enhancing or modifying the photophysical properties of the

to elicit new radiative recombination pathways, such as type II or charge-transfer photoluminescence (PL),^[3] or modify multi-exciton recombination processes.^[4] Finally, the heterostructure combining a type II electronic structure with a thickened or “giant” shell has been shown to lead to dramatically improved

Prof. A. M. Dennis
Department of Biomedical Engineering and Division of Materials
Science and Engineering Boston University
Boston, MA 02215, USA
Prof. M. R. Buck
Department of Chemistry
United States Naval Academy
Annapolis, MD 21402, USA

 The ORCID identification number(s) for the author(s) of this article can be found under <https://doi.org/10.1002/adfm.201809111>.

^[†]Present address: Laboratory for Advanced Materials, Faculty of Natural Sciences, Comenius University, 84 215 Bratislava, Slovakia

Dr. F. Wang, Dr. N. F. Hartmann, Dr. S. Majumder, Dr. J. L. Casson,
Dr. J. D. Watt, Dr. S. K. Doorn, Dr. H. Htoon, Dr. J. A. Hollingsworth
Center for Integrated Nanotechnologies
Materials Physics and Applications Division
Los Alamos National Laboratory
Los Alamos, NM 87545, USA
E-mail: jenn@lanl.gov
Dr. M. Sykora^[†]
Chemistry Division
Los Alamos National Laboratory
Los Alamos, NM 87545, USA

DOI: 10.1002/adfm.201809111

photostability at the level of single QDs, with respect to both reduced blinking and photobleaching.^[5]

Colloidal nanocrystal QDs that exhibit type II band alignment predominantly comprise combinations of II–VI semiconductors. Examples of III–V compounds exhibiting type II band alignment, such as InP/GaAs and GaSb/GaAs, are found primarily in the literature for self-assembled QDs, prepared by molecular beam epitaxy or chemical vapor deposition.^[6] By combining InP, a III–V compound, with CdS, a II–VI compound, we showed previously that colloidal InP/CdS core/shell QDs possessed a type II band alignment, such that emission arose from interfacial carrier recombination rather than recombination in either the core or the shell. This was indicated by emission energies that were less than the bulk bandgap energy of InP or CdS (PL \approx 1.25 eV; \approx 990 nm, compared to the InP bandgap of 1.34 eV; 925 nm, or the CdS bandgap of 2.4 eV; 515 nm). Clear type II emission (energies less than the component bulk bandgap energies) in the case of InP/CdS was realized specifically for relatively thick shells – \approx 2.75 nm or \approx 8 CdS monolayers (MLs).^[5c] InP/CdSe has also been reported as a type II QD,^[7] but in that case shell growth was limited to thin CdSe layers (<4 MLs), and the emission that was described as type II only reached 1.77 eV (700 nm). In contrast, here we show that near-infrared (NIR) PL in the InP/CdSe system can indeed surpass the “red limit” afforded by the bulk bandgap of InP and, thus, is definitively type II in nature. Furthermore, such NIR PL onsets at thinner shells compared to the InP/CdS system. For InP cores similar in size to those used in our report on InP/CdS QDs, we show here that the addition of only \approx 1.4 nm (\approx 4 ML) of CdSe shell yields PL centered at 1.28 eV (970 nm).

In addition to validating the type II behavior of InP/CdSe QDs, we demonstrate emergence of a new phenomenon for III/V QDs—two-color excitonic emission, where type II NIR emission and type I visible emission occur simultaneously, with the latter originating from the shell. Dual emission in II/VI nanostructures is known and has been produced as an effect of either composition or structure. QDs and nanorods that are chemically doped with transition metal impurity ions can exhibit emission from both the host semiconductor and the dopant ions if the semiconductor excitonic states are tuned to lie just above the lowest excited state of the dopant ion, where they are thermally accessible.^[8] Alternatively, heterostructuring the nanocrystal to include a potential energy barrier layer between two potentially emissive regions, e.g., between a core and an outer shell, slows or prevents electron and/or hole tunneling, also affording two-color emission.^[9] Finally, extreme asymmetry of the nanocrystal shape, such as realized in core/arm tetrapods, can result in two-color emission at high excitation fluences.^[5b,10] In this case, dual emission is a multi-exciton process that depends on concurrent suppression of non-radiative Auger recombination processes in the arms that is enabled by arm lengthening.^[5b] Thus, doping, heterostructuring, and shape control are synthetic parameters that have been used to influence the fate of excitons (and multi-excitons) in II–VI semiconducting nanostructures, with potential applications including ratiometric temperature sensing^[8a,d] and white-light generation.^[10a]

Here, we introduce an alternative mode for realizing two-color emission that depends on the sensitivity of InP cores to their chemical treatment prior to shell growth. We further

observe that core/shell heterostructuring can be used to change the probability for of observing dual emission and to stabilize the contributing radiative processes. Specifically, we find that the core/shell interface can be chemically engineered to either yield nanocrystals capable of dual emission or not. In contrast with some other studies for which dual emission has been reported,^[9f,11] we use single-emitter spectroscopy to conclusively show that the two-color PL observed for ensembles of InP/CdSe QDs in solution does indeed originate from emission occurring in single QDs, rather than from the possible presence of two QD populations. At the single-nanocrystal level, we also assess blinking behavior for the two emission processes, identifying the shell characteristics that afford the strongest blinking suppression.

2. Results and Discussion

We demonstrated previously that it is possible to grow InP/CdS thick shell or giant core/shell QDs (gQDs) using the layer-by-layer shell-growth technique known as the successive ionic layer adsorption and reaction (SILAR) method.^[5c] In that case, \approx 10 MLs of shell afforded significantly enhanced photostability for the type II InP/CdS emission. To avoid etching of the InP QDs and to lessen the likelihood of core oxidation upon exposure to SILAR growth conditions (basic or acidic ligands, e.g., oleylamine or oleic acid, respectively, and high temperature, e.g., 240 °C), we established a shell-growth protocol whereby an initial ML of shell was added at low temperature (150 °C). A similar approach has now been applied to synthesis of InP/CdSe core/shell QDs, which allowed us to successfully realize similarly thick shells.

Unexpectedly, we show here that CdSe shell growth leads not only to stable type II NIR emission, but also to two-color NIR and red-visible emission. Up to approximately 10 MLs of CdSe were added to InP cores ranging in size from \approx 1.75 to 3.25 nm diameter (Figure 1a–d; transmission electron microscopy (TEM), series shown for starting core diameter of \approx 1.75 nm; Figure S1, Supporting Information: powder X-ray diffraction pattern progression with increasing CdSe shell thickness). In this series, all but the smallest cores were precipitated from their growth solutions prior to shell growth using Ar-sparged methanol/butanol mixture, followed by resuspension in degassed octadecene (ODE). The \approx 1.75 diameter cores were instead subjected to shell growth directly in the QD growth solution (see below for further discussion of the effect of pre-shell-growth core treatment on resulting core/shell spectral properties). Type II NIR PL is clearly visible in the 1.2–1.5 eV range for all shell thicknesses (Figure 1e), while visible emission (1.8–2.0 eV) emerges with >3 –4 ML CdSe (Figure 1e, orange trace). This shell thickness corresponds to a CdSe volume of \approx 50–60 nm³, or the same volume as a 4.6–4.9 nm diameter QD. This study utilized InP cores ranging from 1.75 to 3.25; thus at 3–4 MLs, the CdSe shell comprises $>50\%$ of the total volume of the particle. Having a similar molar extinction coefficient to InP,^[12] it is at this shell thickness that CdSe would be expected to contribute similarly to the QD absorption cross-section. Indeed, a CdSe absorption feature is clearly discernable at shell thicknesses/volumes close to those where shell emission emerges (Figure S2, Supporting Information). Both NIR and visible

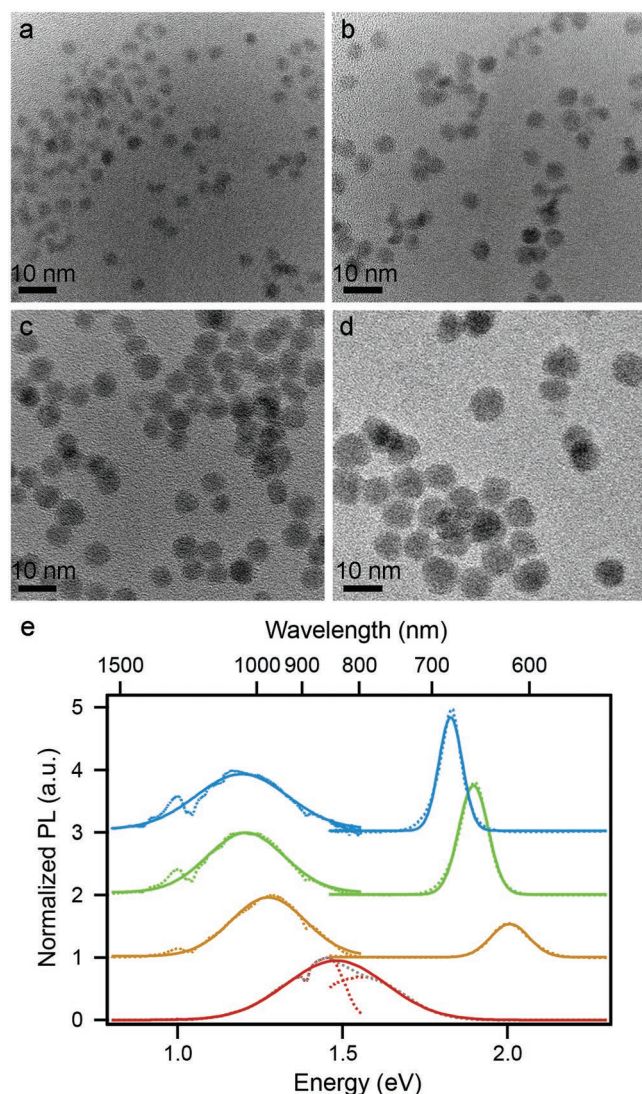


Figure 1. TEM images of InP/CdSe QDs for a representative shell thickness series: a) ≈ 1 ML CdSe, b) ≈ 4 ML CdSe, c) ≈ 7 ML CdSe, and d) ≈ 10 ML CdSe. e) Normalized PL spectra spanning visible and NIR spectral range for the same shell series (progressively from bottom to top). Spectra are offset for clarity. The measurement transitions from the visible to the NIR detector at ≈ 1.5 eV; solvent absorption effects are responsible for the artifact at ≈ 1 eV.

peaks transition to lower energies with increasing shell thickness, with the NIR emission plateauing for CdSe shells thicker than ≈ 2 nm or ≈ 7 MLs (Figure S3, Supporting Information).

Core/shell QDs prepared using the largest core attain longer wavelengths in emission at relatively thinner shells compared to smaller-core counterparts (Figure S3, Supporting Information). For this reason, in Figure 2, we plot visible and NIR PL as a function of shell volume, rather than shell thickness, and find a clear correlation between shell volume and PL peak position. Interestingly, if we compare the observed visible-PL/shell-volume trend obtained for the InP/CdSe QDs with the behavior of CdSe QDs, we find that the CdSe QD visible-PL/particle-volume trend (Figure 2b, aqua triangle series) shows a similar volume dependence at volumes below 100 nm^3 . However, the two emitter types

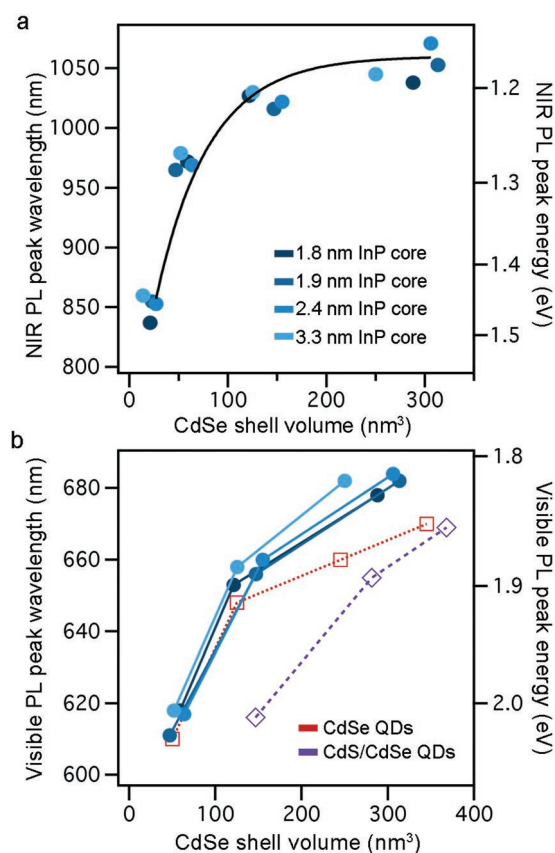


Figure 2. a) NIR and b) visible PL peak wavelengths/energies as a function of CdSe shell volume for an InP/CdSe core-size series. In b), the respective trends for CdS/CdSe shell emission and for CdSe QD emission (sphere volumes in this case) are also shown.

substantially deviate at larger volumes. Very large CdSe QDs (245 and 345 nm^3 volumes, corresponding to QD diameters of 7.8 and 8.7 nm , respectively) exhibit PL peak positions that are less redshifted compared to the emission wavelengths observed for same-volume CdSe shells (Figure 2b red, yellow, blue, and purple circle series above 100 nm^3 shell volumes). This might suggest that the quantum confinement felt by excitons in the shell geometry is relatively less than that in the QD geometry for similar volumes, allowing PL energies to more quickly approach the CdSe bulk bandgap (712 nm ; 1.74 eV).

To test this hypothesis, we compared the InP/CdSe shell-emission behavior with that for CdS/CdSe QDs, which afford exclusively CdSe-shell PL. Contrary to the observation for the InP/CdSe QDs, we find that shell emission in this system is blueshifted from that for either same-volume CdSe shells on InP or same-volume CdSe QDs. Intriguingly, though energetically separated, the slope of PL change as a function of volume change was similar for the two shell emitters. The higher energies observed for emission from CdSe shells grown on CdS cores compared to that from CdSe QDs might be explained by an effect of compressive strain,^[13] which is experienced by a shell that is overgrown onto a material possessing a smaller lattice constant than itself (CdSe zinc blende lattice parameter: 6.08 \AA , compared to CdS: 5.82 \AA). On the other hand, CdSe grown on InP cores should experience a similar mismatch strain, as the

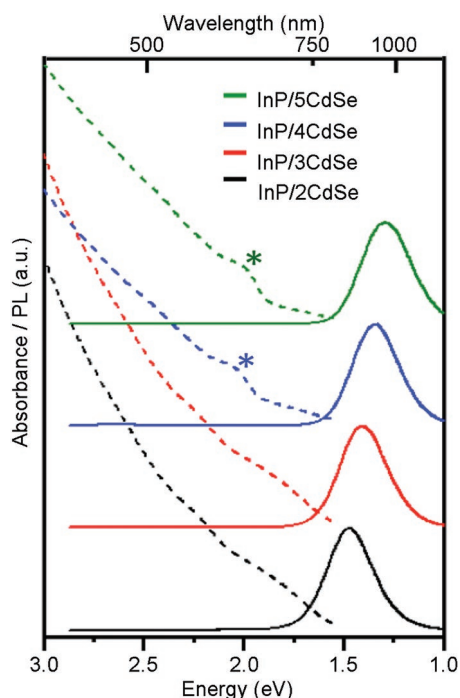


Figure 3. Absorption (dashed) and emission (solid) for a shell thickness series for which visible PL is not observed. A * indicates the CdSe 1S absorbance position.

InP lattice constant is very similar to that for CdS (InP: 5.87 Å). We discuss below other possible explanations for the relatively lower energy PL obtained for the InP/CdSe visible emission.

The treatment of the InP core prior to shell growth plays an important role in the observation of CdSe shell emission. When InP cores are kept rigorously free of air and water during synthesis, purification, and shell growth, we find that it is possible to prevent visible shell emission. Post-synthesis workup was conducted in an inert atmosphere glovebox to prevent rapid oxidation of the InP surface by O_2 .^[14a] Also, In(III) myristate (generated from In(III) acetate) was also replaced with anhydrous $InCl_3$ as the indium precursor (see Experimental Details, Supporting Information) to avoid water that can hydrolyze the phosphine precursor and/or the nanocrystal surface, leading to unintentional incorporation of oxygen. A growing number of studies indicate that surface $InPO_x$ ($x = 2, 4$) form unavoidably during InP preparation when In(III) carboxylate precursors are used, due either to release of water from ketonization side reactions or simply from the hygroscopicity of those precursors.^[14] Avoiding both sources of oxygen results in InP/CdSe QDs that exhibit no detectable CdSe emission, although the CdSe absorbance feature appears as expected around 4 ML CdSe (Figure 3).

To better establish the correlation between oxygen exposure and the observation of dual emission, we intentionally oxidized InP cores prior to shell growth by exposing them to air. Indeed, the resulting core/shell QDs yielded two-color emission (Figure S4a, Supporting Information). Qualitatively, the contribution of visible emission to total core/shell PL intensity agrees with a presumed relative extent of core surface oxidation based on the reaction conditions employed—from visible emission dominating (intentional exposure of InP cores to air;

Figure S4a, Supporting Information) to contributing about half (imperfect “air-free” InP core workup; Figure S4b, Supporting Information) to little (one-pot reaction; Figure S4c, Supporting Information) and to none (rigorously air-free work-up and use of $InCl_3$ precursor; Figure 3) of the total PL. Taken together, these results imply that surface oxidation is a pre-condition for dual emission and that it can be used to tune the relative intensities of shell and type II emissions.

In an attempt to create a pristine InP surface for shell growth and to, thereby, eliminate secondary shell emission at will, we subjected InP cores to photochemical surface etching with HF.^[12b] The previously reported role of HF is to remove undercoordinated P atoms from the InP surface, which leaves the surface In rich.^[15] We surmised that removal of dangling P bonds would create surface vacancies that could be deliberately filled with selenium during SILAR growth of the CdSe shell. However, contrary to our expectation, we found that HF-treated cores reliably exhibited dual emission, rather than preventing its appearance. Thus, core/shell products of HF treated InP behaved similarly to their unintentionally or intentionally oxidized core counterparts. X-ray photoelectron spectroscopy studies by Adam and co-workers^[15] show that it is possible for fluoride or oxygen to occupy the resulting P vacancies. Furthermore, we cannot rule out the possibility of F^- binding directly to surface In atoms, including exchange of native ligands (TOP/TOPO) for F^- . A very recent report suggested that at lower HF exposure, including HF:InP ratios as high as 5000:1 (we used a ratio of 8000:1), surface fluorination, and not etching, was the dominant mechanism by which HF reacts with InP QDs.^[16] In either case the HF process would promote introduction of F or O surface species prior to CdSe shell growth. Below, based on an analysis of ultrafast carrier relaxation processes using the transient absorption (TA) technique, we discuss the role such anionic species adventitiously positioned at the core/shell interface might play in the development of two-color emission, as well as in the above observed redshifting of InP/CdSe shell emission compared to CdS/CdSe shell emission.

A further modification to the QD structure was used to significantly enhance the stability of observed shell emission. Namely, an outer CdS shell layer was added to the InP/CdSe QDs to form InP/CdSe/CdS core/shell/shell QDs [see Figure S5, Supporting Information: progression of nanocrystal structure (TEM) and composition (ensemble energy-dispersive X-ray spectroscopy) with addition of CdS shell]. Without this additional synthetic step, visible emission (especially at lower CdSe MLs) was highly sensitive to post-synthesis work-up, i.e., the precipitation/re-dissolution protocol used to remove excess ligands. (Note: here, workup was extensive, as the free ligands and native solvent, ODE, are aliphatic hydrocarbons and, as such, strongly absorb in the NIR region where InP/CdSe QDs emit; thus, their removal and the subsequent transfer of the QDs to, e.g., tetrachloroethane, was essential for obtaining high-quality spectra in the NIR). Without addition of a CdS shell, the NIR:visible PL intensity ratio was observed to increase, for example, from ≈ 4 prior to washing to ≈ 160 after washing (e.g., in the case of a 3.6 nm HF-etched InP/4 ML CdSe QD). The change in relative intensities resulted from a diminishment of visible emission rather than any significant increase in NIR emission. Significantly, addition of increasingly

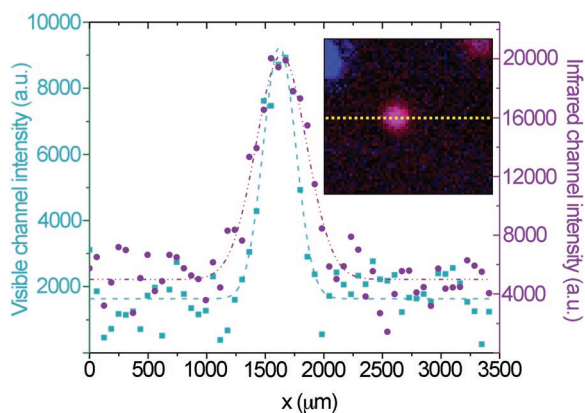


Figure 4. Cross-section through visible and infrared channels showing respective PL intensities from the single InP/5CdSe/5CdS QD displayed in the center of the inset image. Inset: magenta color in widefield image derives from an overlap of blue (visible channel emission) and red (NIR channel emission). QDs emitting only one color are colored either blue or red.

thick CdS secondary shells afforded progressively less sensitivity to washing (Figure S6, Supporting Information).

Relying exclusively on ensemble PL measurements to ascribe the observation of two-color emission to a particular nanoscale structure discounts the possibility that two distinct nanocrystal populations might exist in the collection of nanostructures, each affording one of the observed emission colors. For this reason, we also investigated PL behavior at the level of single nanocrystals. In order to simultaneously observe visible and NIR emission from single QDs, we used either of two configurations— a) wide-field imaging where the two-color channels were recorded using separate electron multiplying charge-coupled device (EMCCD) cameras preceded by a visible or an infrared bandpass filter, or b) confocal imaging where 680 nm short-pass and 720 nm long-pass filters were placed in front of two different silicon avalanche photodiode (APD) detectors to detect visible and NIR emission, respectively. In either case, dual-channel scanning/detection allowed us to identify emissive spots that radiated strongly at both the short and the long bands (Figure 4) and to obtain temporally overlaid PL intensity-time traces (see Experimental Details in Supporting Information and Figure S7).

Once dual emission was confirmed, PL time traces were obtained and analyzed for each emission color separately by placing the same spectral filter (either the short pass or the long pass) in front of each APD. Figure 5 shows representative single-QD PL intensity-time traces, PL decay-time trajectories, and second-order photon correlation functions ($g^{(2)}(0)$) separately obtained for the visible and infrared emissions for representative InP/10CdSe (Figure 5a) and InP/5CdSe/7CdS (Figure 5b) QDs. In addition to spectral filtering, the two emissions were identifiable by their respective average radiative lifetimes, i.e., visible-PL lifetimes fell in the range 25–50 ns (shell thickness and composition dependent) and NIR-PL lifetimes were observed to be ≈ 300 ns for an InP/CdSe QD CdSe shell-thickness series (4, 7, and 10 MLs CdSe) and ≈ 115 –300 ns for an InP/5CdSe/1–7CdS shell series. The observation of $g^{(2)}$ values ≤ 0.5 confirms the single-nanocrystal nature of the QD being interrogated (Figure 5, right). We attribute the fact that the $g^{(2)}$ values are not closer to

0, as would be expected for fully antibunched emission, to the negative effect of a rather large background noise on the $g^{(2)}$ determination, as well as to the possibility that biexciton emission is efficient. The latter would be consistent with our previous observations for CdSe/CdS gQDs, for example.^[17]

As described, inclusion of an outer CdS shell improves visible-emission stability at the ensemble level, but it also strongly influences single-QD properties. For example, the probability of locating QDs possessing dual-emission character is strongly enhanced in the case of thinner CdSe shells (4–5 ML) by growth of even a thin CdS shell (1 ML), e.g., from 15% to $> 70\%$ for InP/4CdSe QDs compared to InP/5CdSe/1CdS QDs, respectively. The failure of the InP/4CdSe sample to exhibit two-color PL was due to a lack of short-band emission. For single-QD analysis, the QDs are subjected to extreme dilution in a dispersal solvent in order to reach the required very low densities on the glass substrate (≈ 1 QD/ $4 \mu\text{m}^2$ area). This process affords similar surface-ligand disruption as does the extensive washing procedure described above. In this way, without the added protection of an CdS overcoating, these InP/thin-CdSe QDs lose the ability to emit visible shell-based emission. Though less dramatically, this trend continues for thicker shells, with CdS-terminated QDs more likely to exhibit dual emission for similar total shell thicknesses (e.g., comparing InP/5CdSe/5CdS and InP/10CdSe in Figures S6 and S7, Supporting Information, respectively).

Growth of a thicker CdSe shell or addition of a CdS outer shell leads to blinking suppression. Visible emission exhibits shell-thickness-dependent blinking suppression, as shown in Table 1 and Figures S6 and S7 in the Supporting Information. NIR blinking is strongly suppressed ($>85\%$ on-time) above total shell thicknesses of ≈ 6 ML. Significantly, both types of shells show blinking-suppressed behavior for each type of emission (NIR and visible) at these thicker shells; however, overall, the gQDs with added CdS shell exhibit enhanced two-color blinking suppression based on analysis of the Mandel Q parameter. Namely, the percentage of QDs having $Q < 3$ (a value indicating strong blinking suppression; see Supporting Information for an explanation of the derivation of this parameter) is highest for InP/5CdSe/7CdS gQDs compared to QDs with thinner CdS shells (Figure 6). Similarly, the percentage of QDs having $Q > 10$ (a value indicating minimal blinking suppression) is at its lowest for the thickest CdS shell. This is the case for the InP/5CdSe/7CdS gQDs for both visible and NIR emissions (Figure 6a,b). A similar shell-thickness trend is evident also for the series of InP/ n CdSe QDs (without an outer CdS shell) in the case of NIR emission, but a positive trend with increasing shell thickness is less clear for visible emission, for which $Q < 3$ is not enhanced between 7 and 10 ML, and data for thinner shells is too sparse to be definitive (Figure S10, Supporting Information). Thus, similar to the effect of a thick CdS shell on CdSe QD emission in the case of CdSe/CdS gQDs,^[5d,f,g] addition of a thick CdS shell onto InP/CdSe QDs suppresses blinking of the CdSe shell PL. We note that the Mandel Q parameter differentiates the two types of QDs more clearly than considering on-time percentages alone, as this parameter takes into account both PL fluctuations between on and off states and between different levels of “on,” i.e., flickering between bright and dimmer states (see Figure S11, Supporting Information for

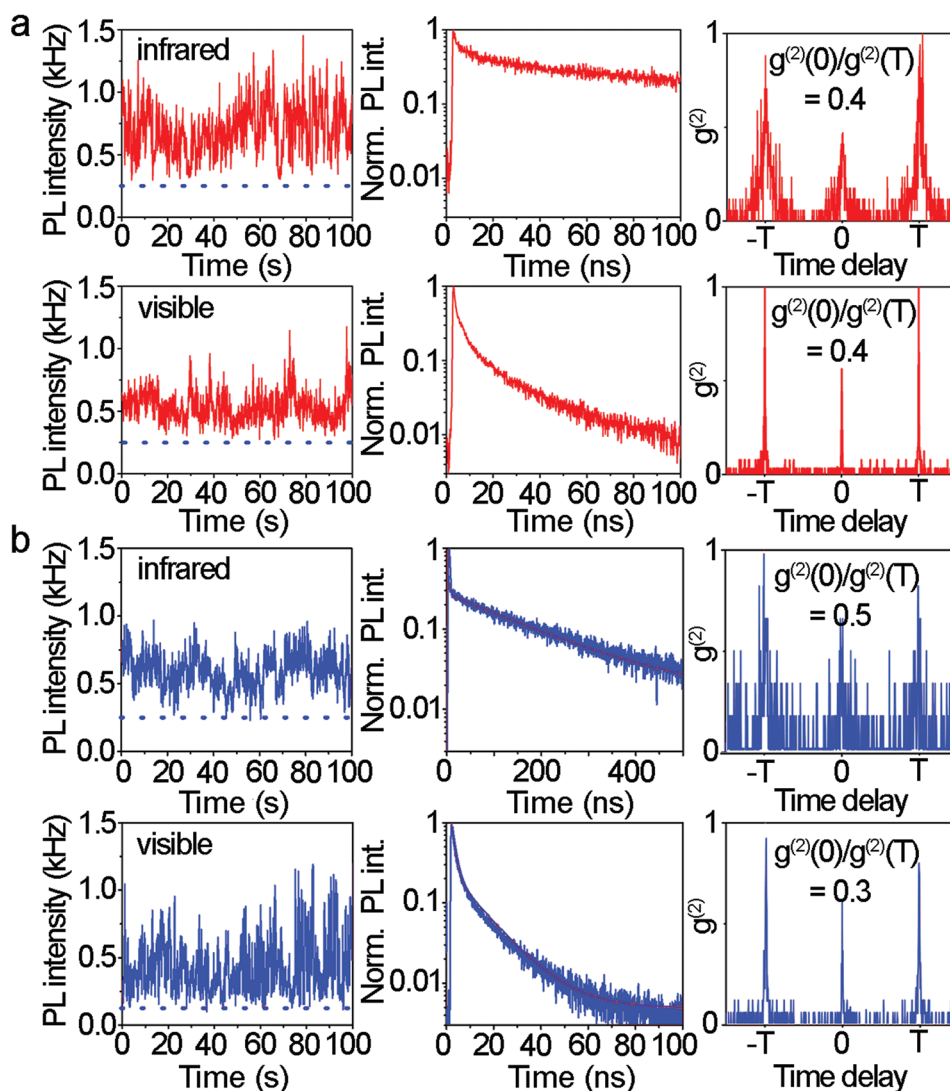


Figure 5. Representative single-QD optical data for a) an InP/10CdSe gQD and b) an InP/5CdSe/7CdS gQD. Wavelength-specific PL intensity-time traces (left), PL decay-time trajectories (middle), and second-order photon correlation functions (right) are shown for each gQD.

a comparison of an InP/5CdSe/5CdS QD with an InP/10CdSe QD, for which similar high blinking on-time percentages but different Mandel Q values are obtained).

Table 1. Shell-dependent blinking statistics for InP/CdSe and InP/CdSe/CdS QDs.

QD	On-time (%) NIR	On-time (%) visible ^{a)}
InP/4CdSe	56	58
InP/7CdSe	86	78
InP/10CdSe	95	90
InP/5CdSe/1CdS	82	69
InP/5CdSe/3CdS	96	78
InP/5CdSe/5CdS	90	85
InP/5CdSe/7CdS	86	95

^{a)}Value is that obtained for the QDs that exhibited visible emission and does not reflect the observation that the majority of InP/4CdSe QDs, for example, did not exhibit dual emission.

A question remains as to whether the two emissions are electronically coupled. The fact that their respective lifetimes are distinct and accurately reflective of their likely origins, i.e., type II NIR PL exhibits significantly slower decay compared to type I shell emission, suggests they are uncoupled emitters.^[9d] Furthermore, PL intensity time traces collected simultaneously (Figure S7, Supporting Information) reveal that intensity

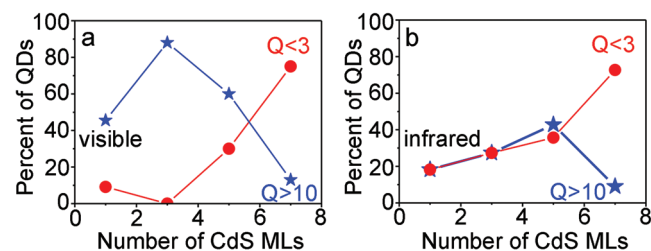


Figure 6. InP/CdSe/CdS Mandel Q parameters as a function of number of CdS MLs.

fluctuations for the NIR and visible emissions do not appear correlated. That said, higher temporal resolution would be required to confirm that no correlation is present. At low excitation levels (<1 electron–hole pair per laser pulse), it might be expected that visible shell emission would prevent observation of NIR type II emission, and vice versa.

If a competitive relationship between the two types of emission exists, then in the least a negative correlation should exist, such that visible shell emission would preclude observation of NIR type II emission, and vice versa, at low excitation levels (<1 electron–hole pair per laser pulse). Namely, when an exciton is formed in the shell, which dominates emission in the case of thick shells, for NIR type II PL to occur the hole must relax to the lower energy valence band state in the InP core, while the electron remains in its lowest lying conduction band state in the CdSe shell. Interfacial, type II carrier recombination then takes place with emission of an NIR photon. The observation of visible shell emission suggests that hole shell-to-core relaxation is somehow impeded, allowing electron–hole recombination in the shell to compete with, and sometimes effectively circumvent, type II emission. In contrast, core-to-shell electron relaxation, in the case of core excitation, is not hampered, as no InP core emission is observed for any shell thickness.

Dual emission in spherical core/shell nanocrystals has been attributed to the existence of electron and hole (CdSe/ZnS/CdSe)²⁷ or exclusively hole^[9b–d] barriers within the nanostructures, as well as to the effect of an abrupt core/shell interface where there is a large change in valence band energy levels between core and shell.^[11] The latter explanation is likely not relevant to the InP/CdSe system, as we are able to turn dual emission on or off as a function of chemical treatment of the core. Significantly, this observation strongly suggests that any explanation relying on the “intrinsic” properties of the core/shell system does not apply here. Instead, we suggest that surface changes to the InP core by adventitious or intentional oxidation, or as a result of HF treatment, introduces either a barrier to hole relaxation or, as an entirely alternative explanation, an impurity or defect state. We speculate that a defect of anionic character could create a barrier or provide a shallow energetic trap near the valence band edge of the shell that could prevent the hole from effectively migrating into the InP core. In this way, the trapped hole could succumb to either of two processes—relaxation to the core and type II recombination or direct recombination with an electron in the shell.

To distinguish between these two possibilities, we performed ensemble TA measurements on InP/CdSe samples that exhibited distinct PL behaviors, namely InP/5CdSe QDs that exhibited either NIR-only emission (rigorously air-free synthesis; 3.6 nm diameter InP), sample A, and dual emission (InP core HF etched prior to CdSe shell growth; 3.5 nm diameter InP), sample B. The results for the time range 2–100 ps after excitation at 400 nm (3.1 eV) are summarized in **Figure 7**. In both core/shell samples, the visible TA signal is dominated by a prominent bleach with a peak at ≈ 620 nm. A comparison with an InP control sample (**Figure 7e**) indicates that although the bleach of the control has a peak at a similar wavelength (≈ 640 nm) both the magnitude and the shape of the bleach signal are different from those of the core/shell structures. Therefore, we conclude that the visible TA bleach in the core/shell structures is dominated by electrons

located in the CdSe shell, with the CdSe shell bandgap being coincidentally similar to the bandgap of the InP core. (Note: in CdSe the TA signal is primarily sensitive to electrons^[18]). Three distinct features, labeled b_1 , b_2 , and b_3 , in the bleach of the samples A and B are correspondingly assigned to the $1S(e)-1S_{3/2}(h)$, $1S(e)-2S_{3/2}(h)$, and $1P(e)-2P_{3/2}(h)$ transitions in the CdSe shell.^[19] Compared to the visible signal, The NIR TA signal (**Figure 7b,d**) comprises a relatively weak bleach that appears at wavelengths < 1000 nm and a weak induced absorption above 1000 nm. This is the case for both core/shell samples. Based on the PL results and general understanding of type II core/shell structures, we assign the NIR bleach at ≈ 850 nm to type II electron–hole recombination between the CdSe shell and the InP core. Closer examination of the shape of the spectra in this region reveals noticeable differences in the signal of the two core/shell samples (**Figure 7b,d** insets). Namely, while sample A shows distinct bleach in this range, the bleach is almost absent in sample B.

Further insight into the mechanism of the carrier recombination can be obtained from inspection of the bleach relaxation dynamics. Comparison of bleach signals in the visible range shows that the magnitude of the bleach for samples A and B at ≈ 2 ps (i.e., after initial thermal carrier relaxation) is very similar ($\Delta\alpha/\alpha_{\text{exc}} \approx 35\text{--}38$ mOD at peak of the main b_1 feature). This observation indicates that there is a similar number of electrons available at the CdSe conduction band edge after the initial carrier “cooling” period. However, after ≈ 2 ps the bleach relaxation dynamics is distinct for samples A and B. In sample A the main bleach feature, b_1 , relaxes with time constant $\tau \approx 91$ ps (**Figure 7a,f**). This time constant is similar to the relaxation of the bleach feature at ≈ 850 nm ($\tau \approx 80$ ps), suggesting that relaxation dynamics of the two features is controlled by the same process, namely recombination of electrons in the CdSe shell with holes in the InP core.

In contrast, in sample B, the b_1 feature of the visible bleach decays more rapidly, with time constant $\tau \approx 60$ ps (**Figure 7b,g**), while the very weak signal at 850 nm undergoes significantly smaller change. This suggests that in this case the fast relaxation of the electrons in the CdSe shell is not significantly coupled to the InP core, i.e., that the fast relaxation of visible bleach in sample B is primarily a CdSe shell-localized process. Indirectly, this observation also suggests that in sample B holes remain primarily localized in the CdSe shell, rather than relaxing to the InP core. A less efficient hole migration from shell to core in sample B could permit shell-localized visible PL to compete with type II recombination and NIR PL, affording the opportunity for the two emission processes to be observed from a single nanocrystal (**Figure 7h**), as we have shown here.

More insights into the nature of the differences in the relaxation of the holes in samples A and B can be obtained by a closer examination of the relaxation dynamics of the individual features, b_1 , b_2 , and b_3 in the visible bleach. In sample A, the b_2 feature is completely relaxed in less than 50 ps. In contrast, within 100 ps, the feature b_3 is relaxed by $\approx 50\%$ (≈ 18 to 9 mOD), while feature b_1 is relaxed by only $\approx 20\text{--}30\%$ (≈ 38 to 28 mOD). Based on the assignments given above, the features b_1 and b_3 are associated with the transitions involving hole states close to the valence band edge (**Figure 7h**). The slow relaxation of these features then suggests that these states have been very rapidly depleted of hole populations, likely due

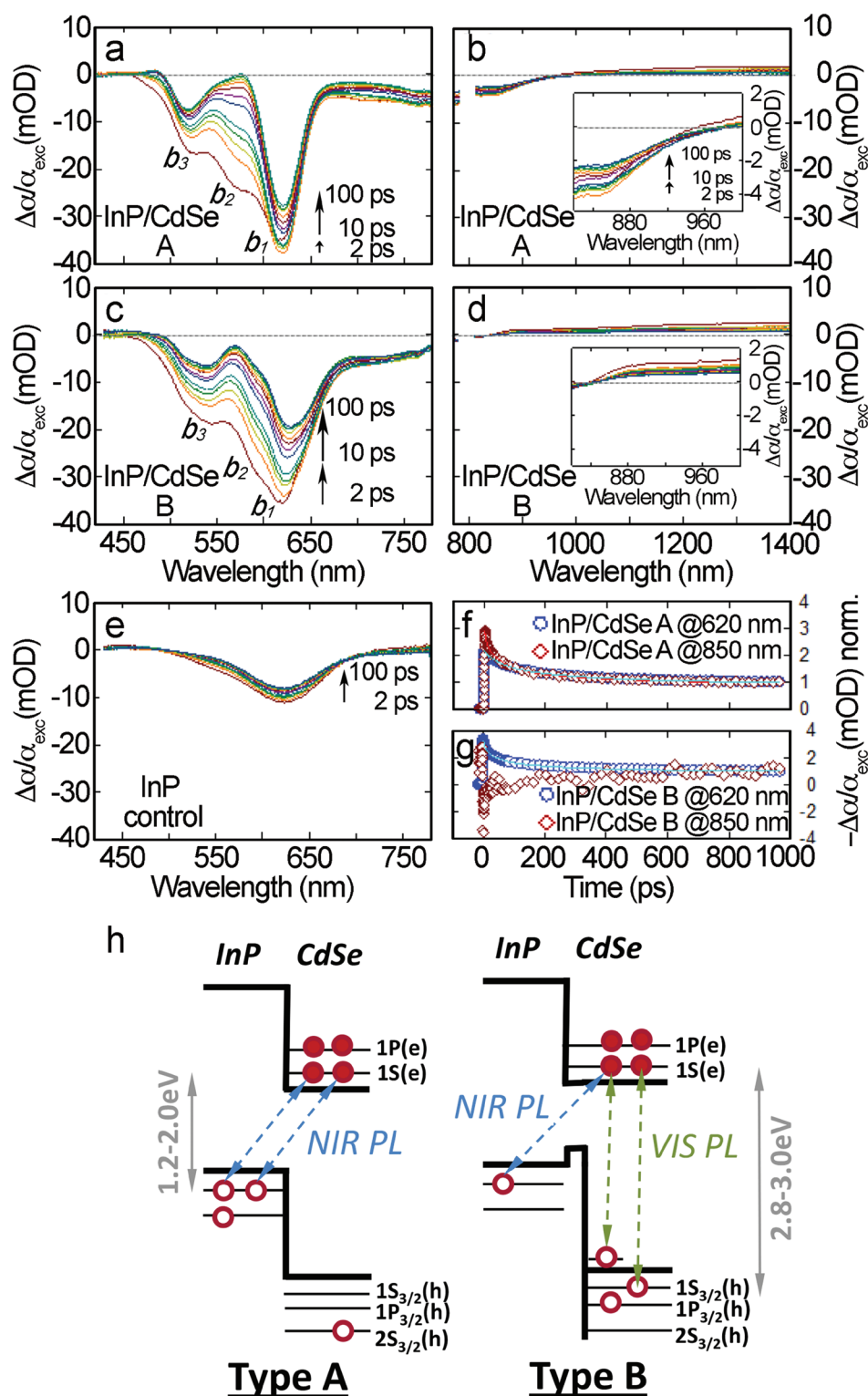


Figure 7. TA spectra for a,c,e) visible and b,d) NIR spectral ranges. TA kinetics for f) NIR-emitting InP/CdSe sample A and g) dual-color emitting InP/CdSe sample B. h) Energy diagrams illustrating (left) the carrier recombination process resulting in infrared type II PL or (right) the case where visible emission in the shell is competitive with type II PL to yield dual-color emission.

to their migration into the InP core. The rapid relaxation of the b_2 feature, involving $2S_{3/2}(h)$ state (further from the band edge) suggests that electron-hole recombination involving

this state takes place within the shell, prior to the hole migration to the CdSe band edge (no visible PL) and into the InP core. The relaxation dynamics of the bleach in sample B is

quite different. All three features decay with approximately the same rate. This suggests that most of the holes can effectively recombine with the electrons in the CdSe shell, i.e., the diffusion of holes into the InP core is inhibited. This observation is consistent with the presence of a hole potential energy barrier at the core/shell interface, as has been implicated previously in systems with intentionally synthesized tunneling barriers,^[9b,d,f] or the combination of an energetically abrupt interface and a thick shell, though this has only been shown to afford a very weak shell emission.^[11] The additional factor that has been proposed to inhibit shell-core migration of carriers is the formation of hole trap states arising from the presence of impurity ions or unpassivated constituent atoms.^[20] In the case of InP/CdSe core/shell QDs, the latter could introduce states within the bandgap of the CdSe shell (Figure 7h, right). Given growth conditions employed here, these would likely be located at or near the core/shell interface, such as the F or O species discussed above, and would, thereby, promote localization of a hole in the vicinity of shell-localized electrons. Interestingly, the visible TA bleach (most notable in b_1 feature) in sample B is accompanied by a redshift of ≈ 10 nm on the time scale of 100 ps. This is not observed for sample A. We tentatively attribute this redshift to a migration of a hole into a shallow hole trap. The TA bleach and PL resulting from recombination between a hole trapped in an interface state and a band edge shell electron are expected to be red-shifted relative to the signals obtained from the recombination of carriers localized in band-edge states (Figure 7h, right). Such an origin of the visible emission might also explain the further observation that the Stokes shift between absorption and PL energies is relatively large (≈ 25 – 35 nm) for the InP/CdSe dual emitters compared to that which is typical of CdSe QDs (≈ 10 – 15 nm), as well as why shell emission in the case of InP/CdSe QDs is redshifted compared to that observed for CdS/CdSe QDs.

3. Conclusion

Core/shell heterostructuring provides a powerful platform for engineering band structure and modifying carrier recombination processes in colloidal semiconducting nanocrystals. Compared to II–VI compounds, however, the approach has been employed to a lesser extent in the case of III–V QDs. Here, we have demonstrated by analysis of PL energy trends and using TA spectroscopy that InP/CdSe core/shell QDs exhibit properties consistent with type II band alignment. More significantly, we have shown that the susceptibility of the InP surface to incorporation of oxygen or other impurity ions, though generally detrimental to InP QD QY, can be utilized for initiating simultaneous type II radiative recombination and CdSe shell emission. The ratio of the two colors in the dual-band PL was found to be fully tunable by controlling various synthetic parameters—the extent of oxygen exposure during InP core workup, the choice of In(III) precursor compound (presence or absence of trace water), and/or the use of HF etching, which has the effect of introducing anionic impurities.

The necessary condition for two-color emission is suppression of hole relaxation to the InP core. This can be caused by

the presence of an energy barrier at the core/shell interface, as has been reported for core/barrier-shell/shell dual-emitting QDs that employ intermediate shells as thick tunneling barriers.^[9] However, here, no intentional intermediate shell was grown. Also, employed synthetic conditions would be expected, at most, to incorporate oxygen at sub-ML levels, thereby ruling out the inadvertent formation of an InO_x barrier shell. For this reason, and the observations of: an anomalous redshift in shell PL compared to CdS/CdSe shell emission, a larger-than-anticipated Stokes shift, and a redshift in visible TA bleach, we propose, instead, that hole relaxation is impeded by trapping to interfacial impurity states. From a shallow trap state, the hole can relax further to the core, or recombine radiatively with a shell-localized electron. In this way, interfacial traps in InP/CdSe QDs provide a new mechanism for breaking Kasha's rule and allowing two colors of light to be emitted from a single structure.

Finally, we further show that shell engineering can lead to strongly suppressed PL fluorescence intermittency. In this case, a very thick CdSe shell or CdSe/CdS multishell (≈ 10 total shell MLs) can be used to achieve essentially non-blinking behavior. The inclusion of CdS as an outer shell has the added effect of stabilizing visible shell emission against the consequences of ligand stripping resulting from washing or extreme dilution, which dramatically increases the likelihood of observing dual emission in single nanocrystals. By analyzing the Mandel Q parameter, we further find that NIR-PL flickering, or fluctuation between bright and dim (gray) states, is reduced by addition of a thick shell of either composition. In the case of visible PL, application of an outer CdS shell affords the clearest enhancement of PL quality. In this way, the InP/CdSe/CdS heterostructure is the most amenable to taking advantage of the synthetically accessible and tunable dual emission behavior and realizing stable, blinking-suppressed type II NIR and shell-localized visible emissions in single colloidal III–V QDs.

Supporting Information

Supporting Information is available from the Wiley Online Library or from the author.

Acknowledgements

A.M.D. and M.R.B. contributed equally to this work. The work was supported by a Division of Materials Science and Engineering, Office of Basic Energy Sciences (OBES), Office of Science, U.S. Department of Energy (DOE) grant no. 2009LANL1096. M.S. was supported for TA studies by the Laboratory Directed Research and Development (LDRD) program at Los Alamos National Laboratory. S.M. was funded for developing new CdSe architectures by the U.S. Department of Energy division of Energy Efficiency and Renewable Energy (EERE), grant no. M615002955. Work was performed primarily at the Center for Integrated Nanotechnologies, a DOE, OBES Nanoscale Science Research Center & User Facility, with aspects of the work supported by a CINT User Project (2016AU0079).

Conflict of Interest

The authors declare no conflict of interest.

Keywords

dual emission, giant quantum dots, nanoscale engineering, suppressed blinking

Received: December 21, 2018
Revised: April 30, 2019
Published online:

- [1] J.A. Hollingsworth, *Chem. Mater.* **2013**, 25, 1318.
- [2] a) M. Chern, T.T. Nguyen, A. H. Mahler, A. M. Dennis, *Nanoscale* **2017**, 9, 16446; b) J. Kundu, Y. Ghosh, Y. A. M. Dennis, H. Htoon, J. A. Hollingsworth, *Nano Lett.* **2012**, 12, 3031; c) E. A. Dias, S. L. Sewall, P. Kambhampati, *J. Phys. Chem. C* **2007**, 111, 708.
- [3] a) C.-H. Chuang, S. S. Lo, G. D. Scholes, G. C. Burda, *J. Phys. Chem. Lett.* **2010**, 1, 2530; b) S. A. Ivanov, A. Piryatinski, J. Nanda, S. Tretiak, K. R. Zavadil, W. O. Wallace, D. Werder, V. I. Klimov, *J. Am. Chem. Soc.* **2007**, 129, 11708; c) S. Kim, B. Fisher, H.-J. Eisler, M. Bawendi, *J. Am. Chem. Soc.* **2003**, 125, 11466.
- [4] D. Oron, M. Kazes, U. Banin, *Phys. Rev. B* **2007**, 75, 035330.
- [5] a) C. J. Hanson, N. F. Hartmann, A. Singh, X. Ma, W. J. I. DeBenedetti, J. L. Casson, J. K. Grey, Y. J. Chabal, A. V. Malko, H. Htoon, J. A. Hollingsworth, *J. Am. Chem. Soc.* **2017**, 139, 11081; b) N. Mishra, N. J. Orfield, F. Wang, Z. Hu, S. Krishnamurthy, A. V. Malko, J. L. Casson, H. Htoon, M. Sykora, J. A. Hollingsworth, *Nat. Commun.* **2017**, 8, 15083; c) A. M. Dennis, B. Mangum, A. Piryatinski, Y.-S. Park, D. Hannah, J. L. Casson, D. J. Williams, R. Schaller, H. Htoon, J. A. Hollingsworth, *Nano Lett.* **2012**, 12, 5545; d) Y. Ghosh, B. D. Mangum, J. L. Casson, D. J. Williams, H. Htoon, J. A. Hollingsworth, *J. Am. Chem. Soc.* **2012**, 134, 9634; e) B. Mahler, N. Lequeux, B. Dubertret, *J. Am. Chem. Soc.* **2010**, 132, 953; f) B. Mahler, P. Spinicelli, S. Buil, X. Quelin, J. P. Hermier, B. Dubertret, *Nat. Mater.* **2008**, 7, 659; g) Y. Chen, J. Vela, H. Htoon, J. L. Casson, D. J. Werder, D. A. Bussian, V. I. Klimov, J. A. Hollingsworth, *J. Am. Chem. Soc.* **2008**, 130, 5026; h) R. Toufanian, A. Piryatinski, A. H. Mahler, R. Iyer, J. A. Hollingsworth, A. M. Dennis, *Front. Chem.* **2018**, 6, 567.
- [6] a) B. Wang, S.-J. Chua, *Appl. Phys. Lett.* **2001**, 78, 628; b) K. Suzuki, R. A. Hogg, Y. Arakawa, *J. Appl. Phys.* **1999**, 85, 8349.
- [7] S. Kim, J. Park, S. Kim, W. Jung, J. Sung, S.-W. Kim, *J. Colloid Interface Sci.* **2010**, 346, 347.
- [8] a) E. J. McLaurin, L. R. Bradshaw, D. R. Gamelin, *Chem. Mater.* **2013**, 25, 1283; b) E. J. McLaurin, M. S. Fataftah, D. R. Gamelin, *Chem. Commun.* **2012**, 49, 39; c) C.-H. Hsia, A. Wuttig, H. Yang, *ACS Nano* **2011**, 5, 9511; d) V. A. Vlaskin, N. Janssen, J. van Rijssel, R. Beaulac, D. R. Gamelin, *Nano Lett.* **2010**, 10, 3670.
- [9] a) Z. Zhang, D. Liu, D. Li, K. Huang, Y. Zhang, Z. Shi, R. Xie, M.-Y. Han, Y. Wang, W. Yang, *Chem. Mater.* **2015**, 27, 1405; b) U. Soni, A. Pal, S. Singh, M. Mittal, S. Yadav, R. Elangovan, S. Sapra, *ACS Nano* **2014**, 8, 113; c) C. Galland, S. Brovelli, W. K. Bae, L. A. Padilha, F. Meinardi, V. I. Klimov, *Nano Lett.* **2013**, 13, 321; d) Z. Deutsch, O. Schwartz, R. Tenne, R. Popovitz-Biro, D. Oron, *Nano Lett.* **2012**, 12, 2948; e) E. A. Dias, A. F. Grimes, D. S. English, P. Kambhampati, *J. Phys. Chem. C* **2008**, 112, 14229; f) D. Battaglia, B. Blackman, X. Peng, *J. Am. Chem. Soc.* **2005**, 127, 10889.
- [10] a) J. I. Wong, N. Mishra, G. Xing, M. Li, C. Sabyasachi, T. C. Sum, Y. Shi, Y. Chan, H. Y. Yang, *ACS Nano* **2014**, 8, 2873; b) A. A. Lutich, C. Mauser, E. Da Como, J. Huang, A. Vneski, D. V. Talapin, A. L. Rogach, J. Feldmann, *Nano Lett.* **2010**, 10, 4646.
- [11] Q. Lin, N. S. Makarov, W.-K. Koh, K. A. Velizhanin, C. M. Cirloganu, H. Luo, V. I. Klimov, J. M. Pietryga, *ACS Nano* **2015**, 9, 539.
- [12] a) J. Jasieniak, L. Smith, J. van Embden, P. Mulvaney, *J. Phys. Chem. C* **2009**, 113, 19468; b) D. V. Talapin, N. Gaponik, H. Borchert, A. L. Rogach, M. Haase, H. Weller, *J. Phys. Chem. B* **2002**, 106, 12659.
- [13] a) M. Montazeri, M. Fickenscher, L. M. Smith, H. E. Jackson, J. Yarrison-Rice, J. H. Kang, Q. Gao, H. H. Tan, C. Jagadish, Y. Guo, J. Zou, M. E. Pistol, C. E. Pryor, *Nano Lett.* **2010**, 10, 880; b) N. Skold, L. S. Karlsson, M. W. Larsson, M. E. Pistol, W. Selfert, J. Tragardh, L. Samuelson, *Nano Lett.* **2005**, 5, 1943; c) L. Balaghi, G. Bussone, R. Grifone, R. Hübner, J. Grenzer, M. Ghorbani-Asl, A. Krashennnikov, H. Schneider, M. Helm, E. Dimakis, **2018**, arXiv:1803.10873.
- [14] a) L. Xie, D. K. Harris, M. G. Bawendi, K. F. Jensen, *Chem. Mater.* **2015**, 27, 5058; b) H. Virieux, M. Le Troedec, A. Cros-Gagneux, W. Solo Ojo, F. Delpech, C. Nayral, H. Martinez, B. Chaudret, *J. Am. Chem. Soc.* **2012**, 134, 19701; c) A. Buffard, Dreyfuss, S., Nadal, B., Heuclin, H., Xu, X., Patriarche, G., Mézailles, N., Dubertret, B. *Chem. Mater.* **2016**, 28, 5925; d) E. A. Baquero, H. Virieux, R. A. Swain, A. Gillet, A. Cros-Gagneux, Y. Coppel, B. Chaudret, C. Nayral, F. Delpech, *Chem. Mater.* **2017**, 29, 9623; e) A. Cros-Gagneux, F. Delpech, C. Nayral, A. Cornejo, Y. Coppel, B. Chaudret, *J. Am. Chem. Soc.* **2010**, 132, 18147; f) M. D. Tessier, E. A. Baquero, D. Dupont, V. Grigel, E. Bladt, S. Bals, Y. Coppel, Z. Hens, C. Nayral, F. Delpech, *Chem. Mater.* **2018**, 30, 6877; g) J. L. Stein, W. M. Holden, A. Venkatesh, M. A. Mundy, A. J. Rossini, G. T. Seidler, B. M. Cossairt, *Chem. Mater.* **2018**, 30, 6377.
- [15] S. Adam, D. V. Talapin, H. Borchert, A. Lobo, C. McGinley, A. R. B. de Castro, M. Haase, H. Weller, T. Möller, *J. Chem. Phys.* **2005**, 123, 084706.
- [16] T.-G. Kim, D. Zhrebetskyy, Y. Bekenstein, M. H. Oh, L.-W. Wang, E. Jang, A. P. Alivisatos, *ACS Nano* **2018**, 12, 11529.
- [17] Y.-S. Park, A. V. Malko, J. Vela, Y. Chen, Y. Ghosh, F. García-Santamaría, J. A. Hollingsworth, V. I. Klimov, H. Htoon, *Phys. Rev. Lett.* **2011**, 106, 187401.
- [18] S. Jeong, M. Achermann, J. Nanda, S. Ivanov, V. I. Klimov, J. A. Hollingsworth, *J. Am. Chem. Soc.* **2005**, 127, 10126.
- [19] V. I. Klimov, *J. Phys. Chem. B* **2000**, 104, 6112.
- [20] B. Omogo, J. F. Aldana, C. D. Heyes, *J. Phys. Chem. C* **2013**, 117, 2317.